Chemical Engineering Journal 495 (2024) 153639

Contents lists available at ScienceDirect

Chemical Engineering Journal

journal homepage: www.elsevier.com/locate/cej

# Characteristics and mechanism of low-temperature NO adsorption by activated carbon

Zhongwei Li, Xingyu Yang, Yutong Wang, Hairui Yang, Qiang Song *

*Key Laboratory of Thermal Science and Power Engineering of Ministry of Education, Tsinghua University, Beijing 100084, China*

ARTICLE INFO

*Keywords:*
NO
Activated carbon
Low temperature
Adsorption
Flue gas

ABSTRACT

Activated carbon is widely used to purify flue gas in industries like steel and metallurgy, but its ability to adsorb $NO_x$ at medium to low flue gas temperatures is limited. This study conducted adsorption experiments in different atmospheres within −20 to 30 °C. As the temperature decreased from 30 °C to −20 °C, the $NO_x$ adsorption amount was increased by 4.61 times. Lowering temperature greatly promoted $NO_x$ adsorption. Temperature-programmed desorption experiments determined the amount of $NO_x$ adsorbed through physical adsorption and chemical adsorption. As the temperature decreased from 30 °C to −20 °C, the proportion of physically adsorbed $NO_x$ to total adsorption amount increased from 2.9 % to 45.5 %, and the proportion of physically adsorbed $NO_2$ to total physical adsorption amount increased from 0 to71.6 %. Lowering the temperature benefited NO oxidation and $NO_2$'s adsorption on activated carbon. Desorption curves of chemically adsorbed $NO_x$ indicated that a decrease in temperature does not affect the chemical adsorption pathways of $NO_x$. Physical adsorption of $NO_x$ was studied by density functional theory calculations. $NO_2$ has much stronger physical adsorption than NO and can physically adsorb near saturated carbon atoms, carbonyl groups, ether groups, hydroxyl groups, and lactone groups. At low temperatures, NO is first oxidized to $NO_2$ on activated carbon and then $NO_2$ is adsorbed through both physical and chemical pathways. Modifying the surface of activated carbon to increase hydroxyl, ether, and lactone groups can help enhance its performance of low-temperature $NO_x$ adsorption.

## 1. Introduction

$NO_x$ is an important atmospheric pollutant that can lead to the formation of photochemical smog, acid rain, ozone depletion, and greenhouse effect [1–3]. Industrial flue gas is one of the primary sources of $NO_x$ emissions into the atmosphere, and it requires control measures to mitigate its impact. When the Selective Catalytic Reduction (SCR) denitrification technology commonly installed in coal-fired units is applied to flue gas treatment in other industries such as steel and metallurgy, it faces challenges such as catalyst poisoning, mismatched temperature ranges, poor load adjustment flexibility, and high costs. Carbon-based adsorbents are widely used for the adsorption of gaseous pollutants, such as employed in flue gas treatment to remove $SO_2$. The use of carbon-based adsorbents to control $NO_x$ emissions in the steel and metallurgy industries is promising.

Among carbon-based adsorbents, activated carbon and biochar are commonly used in industrial flue gas treatment. Compared to biochar, activated carbon has advantages such as a larger specific surface area and richer surface functional groups. These features contribute to its superior $NO_x$ adsorption performance. For example, at room temperature, the adsorption capacity of biochar for NO and $O_2$ is only 0.39 mmol/g [4], whereas the adsorption capacity of coconut activated carbon can reach up to 0.99 mmol/g [5]. Therefore, activated carbon attracts more research attention.

Study on NO adsorption by activated carbon is commonly developed at low-medium temperature (20–150 °C). Within this temperature range, activated carbon exhibits weak adsorption of pure NO (<0.01 mmol/g [5–7]), but in the presence of $O_2$, activated carbon shows significant adsorption of NO [5]. According to literature reports, activated carbons such as copper-impregnated activated carbon, sulfur-impregnated activated carbon, bituminous coal-based activated carbon, coconut shell charcoal, and oxygen-enriched coconut shell charcoal have an adsorption capacity for NO ranging from 0.13 to 2.40 mmol/g at 20–50 °C in the presence of $O_2$ [5,8–10]. This is significantly higher than the adsorption capacity of activated carbon for NO when adsorption occurs solely with NO. Li et al.'s study suggests that $O_2$ adsorbs on active

* Corresponding author.
*E-mail address:* qsong@tsinghua.edu.cn (Q. Song).

https://doi.org/10.1016/j.cej.2024.153639
Received 11 April 2024; Received in revised form 21 June 2024; Accepted 29 June 2024
Available online 1 July 2024

sites near hydroxyl functional groups on the surface of activated carbon, oxidizing gaseous NO to $NO_2$. The generated $NO_2$ then adsorbs on saturated carbon atom sites on the surface of activated carbon [11]. The adsorption and transformation of NO on the surface of activated carbon are primarily attributed to the presence of oxygen, leading to a significant increase in NO adsorption capacity. Scholars [4,12] found that biochar impregnated with KOH exhibits significantly enhanced adsorption capacity for NO compared to untreated biochar. This significant improvement is attributed to the introduction of hydroxyl functional groups to the surface of activated carbon during the impregnation process, which promotes NO oxidation and consequently enhances the adsorption of NO by activated carbon.

At medium to low flue gas temperatures, the adsorption mechanism of $NO_x$ on activated carbon is primarily dominated by chemical adsorption. After completing adsorption experiments at 50 °C, Zhang et al. [13] conducted desorption experiments on the activated carbon samples. They considered the $NO_x$ desorbed by purging at the corresponding adsorption temperature as physical adsorption, while the desorbed products at temperatures higher than the adsorption temperature were considered chemical adsorption. Among them, the amount of chemically adsorbed $NO_x$ accounted for 79.5 % of the total adsorption. After completing the adsorption experiments on activated carbon at 150 °C, Xu et al. [14] first used $N_2$ purging at the adsorption temperature to remove physically adsorbed $NO_x$. Then, they conducted temperature-programmed desorption experiments to remove chemically adsorbed $NO_x$. At this temperature, the proportion of chemically adsorbed $NO_x$ to the total adsorption ranged from 55.5 % to 85.0 %. Chemically adsorbed $NO_x$ predominated on the activated carbon. Through In situ DRIFTS experiments conducted by scholars [11,15,16], it was found that activated carbon exhibits C-$NO_2$ and $NO_3^-$ functional groups after adsorbing NO and $O_2$. This indicates the presence of chemically adsorbed $NO_x$ on activated carbon, in the form of C-$NO_2$ and $NO_3^-$ functional groups. Based on the combination of characterization techniques and quantum chemical calculations, Li et al. [11] proposed that NO oxidizes to $NO_2$ on active atoms near hydroxyl functional groups on the surface of activated carbon. The generated $NO_2$ then chemically adsorbs on saturated carbon atoms, forming two types of chemical adsorption configurations: N-down and O-down. Furthermore, the O-down adsorption configuration of $NO_2$ can further convert to $NO_3^-$. $NO_3^-$ and N-down adsorption configuration of $NO_2$ are the main forms of chemically adsorbed $NO_x$ on activated carbon.

Although activated carbon exhibits weak physical adsorption of $NO_x$ in medium to low temperature flue gas, some scholars have researched physical adsorption. Wang et al. [17] used a magnetic separator to magnetize gases to study the effect of magnetized gases on the adsorption of NO on activated carbon. They found that pre-magnetization of gases can promote the physical adsorption of NO on activated carbon, and during the physical adsorption process, $NO_2$ is the main adsorbate. Through quantum chemistry calculation methods, researchers have found that NO can physically adsorb near saturated carbon atoms, Na atoms, and K atoms [18–21], while $NO_2$ can physically adsorb near saturated carbon atoms, pyridine functional groups, pyrrole functional groups, and quaternary nitrogen functional groups [11,22].

At medium to low flue gas temperatures (20–150 °C), when using activated carbon for the simultaneous removal of $NO_x$ and $SO_2$, activated carbon exhibits a greater adsorption capacity for $SO_2$ compared to $NO_x$. Its ability to adsorb $NO_x$ is relatively limited, making it challenging to achieve efficient simultaneous removal of $NO_x$ [23,24]. Wang et al.'s study indicates that when the adsorption temperature decreases from 20 °C to −20 °C, the adsorption activity of activated carbon significantly increases. The adsorption capacity for NO increases by 4.42 mmol/g, which is 2.73 times larger [5]. Additionally, there is a significant increase in the adsorption of $SO_2$ as well. Based on this discovery, China Huaneng Group Co., Ltd. proposed the Cold Oxidation Adsorption Process (COAP) technology, which achieves efficient purification of heavy metals, $SO_3$, and fine particles while lowering the flue gas temperature to below zero through the flue gas cooling tower. This technology utilizes low temperature (−20 °C) adsorption to achieve efficient purification of NO and $SO_2$. Industrial experiments of COAP technology have shown that it can achieve near-zero emissions of pollutants such as NO, $SO_2$, and particulate matter. Optimizing the low-temperature adsorption performance of activated carbon helps further reduce the cost of this technology and promotes the development and application of this innovative technology. Optimization of activated carbon requires the support of systematic studies on low-temperature adsorption behavior and mechanism.

Currently, research on the characteristics and mechanisms of activated carbon adsorbing NO is mainly conducted in the medium to low flue gas temperature range (20–150 °C), with very limited studies in lower temperature ranges. The demonstration operation of COAP technology illustrates that the application of low-temperature adsorption technology in near-zero emissions control has enormous potential. Therefore, this study utilized an isothermal adsorption experiment system to conduct adsorption experiments of activated carbon on NO within the range of −20 to 30 °C, investigating its low-temperature adsorption characteristics. Additionally, a fixed-bed desorption experiment system was employed to conduct segmented temperature-programmed desorption experiments on different adsorption samples, revealing the adsorption pathways of $NO_x$ on activated carbon. Density functional theory calculations were combined to elucidate the physical adsorption forms of $NO_x$ on the surface of activated carbon.

## 2. Method

### 2.1. Experimental

#### 2.1.1. Sample

The activated carbon samples used in the experiments were obtained from Jiangsu JSW Environmental Technology Co., Ltd., China. The activated carbon was degassed at 200 °C for 2 h to remove moisture and desorb volatile organic compounds adsorbed in the pores. It was then packaged in bags and stored for later use. The ultimate analysis and physical properties of the samples are shown in Table 1. The carbon, hydrogen, and oxygen compositions of the samples were measured using an elemental analyzer (EA3000, EuroVector S.p.A., Italy). The sulfur composition of the samples was measured using a sulfur analyzer (5E-AS3200B, Changsha Kaiyuan Instruments Co., Ltd., China). The pore structure of the samples was analyzed using a surface analyzer (ASAP 2010, Micromeritics Instruments Corporation, USA). The specific surface area was calculated by the Brunauer–Emmett–Teller (BET) method, and the total pore volume was recorded at $P/P_0 = 0.99$.

#### 2.1.2. Adsorption and desorption experiments

The adsorption experiments of activated carbon were conducted using an isothermal adsorption experiment system (Fig. 1). The isothermal adsorption experiment system utilizes a quartz U-shaped tube (inner diameter $\varphi$6 mm, length 250 mm) as the reactor. A low-temperature reaction bath (temperature control range: −40 to 99 °C) is used to create the required low-temperature environment for the adsorption experiments. A mixture of ethylene glycol and water in a 1:1 mass ratio serves as the cooling medium for the low-temperature environment. The U-shaped tube is placed in the cooling medium, and the

**Table 1**
Ultimate analysis and physical properties of the sample.

| Ultimate analysis / wt. % | | | | | Specific surface area / $m^2 \cdot g^{-1}$ | Specific pore volume / $cm^3 \cdot g^{-1}$ | Average pore diameter / nm |
|---|---|---|---|---|---|---|---|
| C | H | O | N | S | | | |
| 86.3 | 0.6 | 13.0 | 0.0 | 0.1 | $1.037 \times 10^3$ | 0.520 | 2.005 |

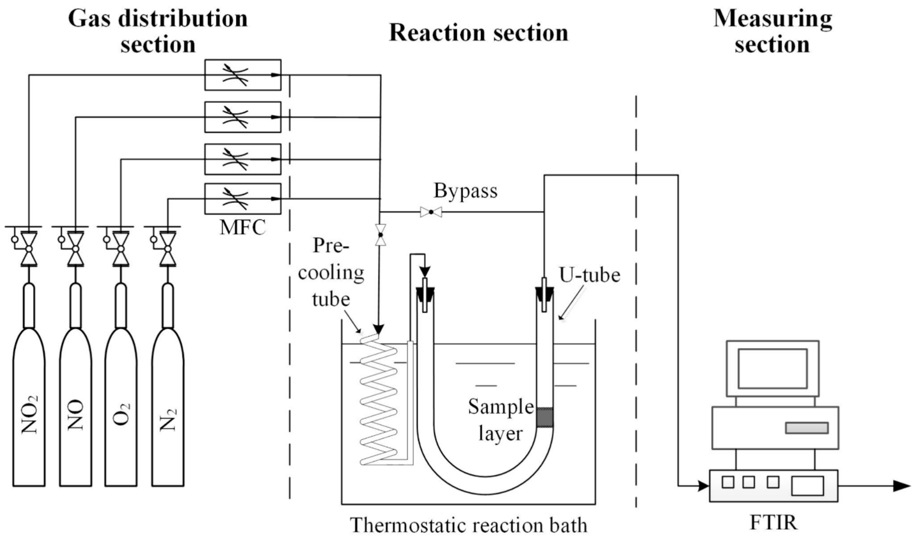


**Fig. 1.** Schematic diagram of the isothermal adsorption experimental system.

activated carbon sample is placed at the lowest end of the straight section of the U-shaped tube. Analytical grade quartz wool plugs are inserted at both ends to ensure that the sample does not move with the flow. 0.1 g of activated carbon sample is loaded into the U-shaped tube, and the temperature of the activated carbon sample is adjusted to the specified temperature *T* by controlling the temperature of the low-temperature reaction bath. The total flow rate of the gas mixture ($NO_2$, NO, $O_2$, $N_2$) entering the reactor is 500 NmL/min. The flow rates of each gas stream are precisely controlled by mass flow controllers. After the gases are mixed, they pass through a spiral pre-cooling tube in the cooling medium to reach the specified temperature *T* before entering the U-shaped tube to begin the adsorption experiment. Fourier Transform Infrared Spectroscopy (FTIR; Nicolet 6700, Thermo Fisher Scientific, USA) is employed to analyze the concentrations of NO and $NO_2$ in the gas exiting the reactor. The measurement error is kept below 3 %. The adsorption experiment concludes either after 120 min of adsorption time or when the concentrations of the gases in the outlet no longer change. To explore the adsorption characteristics of activated carbon on NO in the low-temperature range, three experimental atmospheres are set up: one with a reaction gas of 200 ppm $NO_2$, one with a reaction gas of 200 ppm NO, and one with a reaction gas of 200 ppm NO and 5 % $O_2$. The three experimental conditions are abbreviated as "$NO_2$″, ″NO", and ″NO + $O_2$″. The adsorption experiment conditions are shown in Table 2.

After the adsorption experiments under the three atmospheres, the obtained activated carbon samples are respectively referred to as $AC_{NO_2}$, $AC_{NO}$, and $AC_{NO+O_2}$. Because the maximum temperature achievable by the low-temperature reaction bath is 99 °C, which is insufficient to completely desorb the $NO_x$ adsorbed on the activated carbon, it is necessary to transfer the samples after adsorption to a fixed-bed desorption experimental system capable of reaching higher temperatures for desorption. However, during the transfer of samples, they may come into contact with the ambient air. The temperature difference between the samples and the environment, as well as the difference in

**Table 2**
Adsorption experimental conditions.

| Parameter | Value |
|---|---|
| Amount of AC (g) | 0.1 |
| Temperature (℃) | −20(−20–30) |
| Flow rate (NmL/min) | 500 |
| $NO_2$ (ppm) | 200 |
| $NO_2$ (ppm) | 200 |
| $O_2$ (%) | 5 |

adsorption equilibrium concentrations, may lead to desorption. Therefore, the desorption experiments of the activated carbon samples in this study are divided into the following two stages. Desorption stage 1: After completing the adsorption experiments, the inlet gas of the reactor in the low-temperature reaction bath is switched to $N_2$, and $N_2$ is introduced into the U-shaped tube for purging. During the purging process, the temperature of the low-temperature reaction bath is adjusted to raise the sample temperature from the originally specified adsorption temperature (*T*) to 30 °C. This continues until the sample temperature stabilizes at 30 °C and the concentration of $NO_x$ (NO + $NO_2$) in the outlet gas is below 10 ppm. Desorption stage 1 is then concluded. The $NO_x$ desorbed during this process is mainly attributed to the reduction in the partial pressure of $NO_x$ gases in the atmosphere, leading to the desorption of $NO_x$ weakly adsorbed on the surface of the activated carbon. This portion of $NO_x$ corresponds to physically adsorbed $NO_x$. Desorption stage 2: The activated carbon samples from the completion of desorption stage 1 are transferred to a fixed-bed desorption experimental system for programmed temperature desorption. Nitrogen ($N_2$) is used as the purge gas at a flow rate of 200 NmL/min. The experimental samples are heated from room temperature to 500 °C at a rate of 2 °C/min using a furnace temperature program ($NO_x$ desorption ceases at this temperature). Desorption stage 2 concludes upon reaching this temperature. The desorption curve of $NO_x$ from desorption stage 2 reveals that significant desorption of $NO_x$ begins around 100 °C during the temperature ramping process. This indicates that the main desorbed species during desorption stage 2 are chemisorbed $NO_x$ species.

The fixed-bed desorption experimental system used in this study is shown in Fig. 2. In the figure, the quartz tray is located in the constant temperature zone of the furnace. Its bottom is equipped with quartz sieve plates and high-purity quartz filters (MK360, Munktell, Sweden) for stacking experimental samples. The quartz tray is placed at the top of the quartz inner tube and sealed with ground glass. Other parameters of the fixed-bed desorption experimental system can be found in reference [11]. The airflow enters from the top of the quartz outer tube, passes through the experimental samples, exits from the bottom of the quartz inner tube, and then enters the FTIR for gas analysis.

During the adsorption and desorption experiments, only NO and $NO_2$ nitrogen oxides were detected in the gas at the reactor outlet using FTIR. Based on the changes in NO and $NO_2$ concentrations in the outlet gas over time, the adsorption amount of activated carbon was calculated using Eq. (1), the physical adsorption amount (*T*-30 °C) was calculated using Eq. (2), and the chemical adsorption amount (30–500 °C) was calculated using Eq. (3).

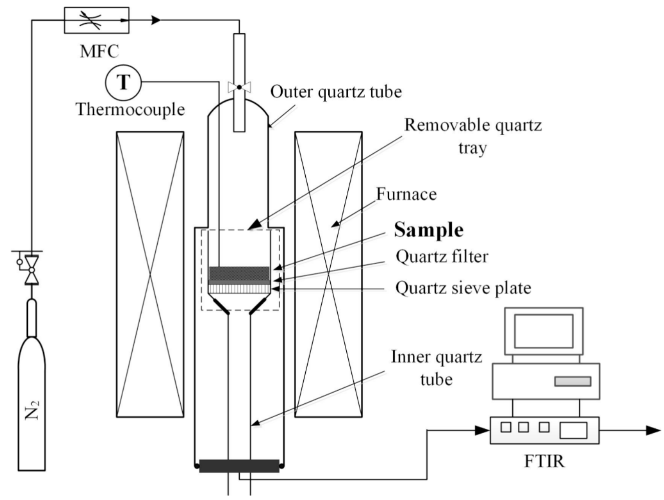


**Fig. 2.** Schematic diagram of the fixed-bed desorption experimental system.

$$N_{NO_x,a} = \int_0^{t_a} \left(\frac{(C_{NO,in} - C_{NO,out} - C_{NO_2,out}) \times 10^{-6} \times Q}{V_m \times m}\right) dt \tag{1}$$

$$N_{NO_x,pa} = \int_0^{t_{pa}} \left(\frac{(C_{NO,out} + C_{NO_2,out}) \times 10^{-6} \times Q}{V_m \times m}\right) dt \tag{2}$$

$$N_{NO_x,ca} = \int_0^{t_{ca}} \left(\frac{(C_{NO,out} + C_{NO_2,out}) \times 10^{-6} \times Q}{V_m \times m}\right) dt \tag{3}$$

where $N_{NO_x,a}$, $N_{NO_x,pa}$, and $N_{NO_x,ca}$ respectively represent the adsorption amount, physical adsorption amount, and chemical adsorption amount of $NO_x$ on the activated carbon (mmol·g$^{-1}$). The integration limits $t_a$, $t_{pa}$, and $t_{ca}$ respectively represent the time required for the completion of adsorption experiments, desorption stage 1, and desorption stage 2 experiments (s). $C_{NO,in}$, $C_{NO,out}$, and $C_{NO_2,out}$ represent the NO concentration in the reactor inlet gas, the NO concentration in the reactor outlet gas, and the $NO_2$ concentration in the outlet gas (ppm), respectively. $Q$ represents the gas flow rate (NmL·s$^{-1}$), $V_m$ represents the molar volume at 0 °C (22.4 L·mol$^{-1}$), and m represents the loading amount of activated carbon (g).

### 2.2. Calculation details

#### 2.2.1. Structural models

XPS characterization was conducted on the activated carbon samples used in this study, and the O1s spectrum is shown in Fig. 3. The spectrum can be resolved into three peaks centered at 531.3–531.3 eV, 532.1–532.3 eV, and 532.2–532.8 eV, corresponding to the carbonyl group (C═O) in ketones, the carbonyl group (C═O) in esters, and the hydroxyl group or ether group (C—O), respectively [10,25]. This indicates that the surface of the activated carbon sample used in this study mainly contains oxygen-containing functional groups, including carbonyl groups, ester groups, hydroxyl groups, and ether groups.

Taking into account the amorphous nature of activated carbon, a typical structural unit of amorphous carbon, namely the carbon cluster model, is constructed. According to references [22,26,27], a carbonaceous model containing 7 aromatic rings is sufficient to neglect the influence of edge effects on computational accuracy. Considering both computational accuracy and efficiency, a pristine carbonaceous model containing 7 aromatic rings is constructed to investigate the low-temperature adsorption mechanism of NO on activated carbon, as shown in Fig. 4a. Based on the XPS characterization of the activated carbon, carbonaceous models containing carbonyl, hydroxyl, lactone, and ether groups were constructed based on the pristine carbonaceous model, as shown in Fig. 4b–e [10,22,27–30]. These carbonaceous models were used to investigate the physical adsorption of $NO_x$ on activated carbon.

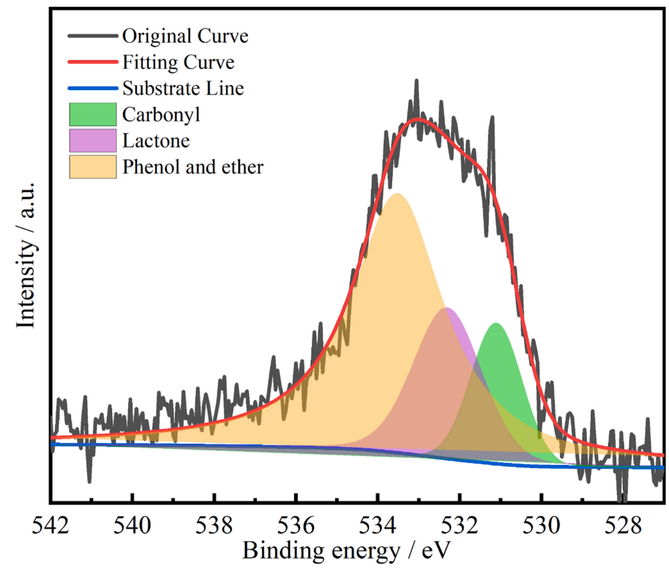


**Fig. 3.** High-resolution O1 s spectra of AC.

#### 2.2.2. Computational methods

All density functional theory (DFT) calculations in this study were performed using Gaussian 16 [31]. Geometry optimizations and frequency calculations were carried out using the B3LYP functional and the 6-31G(d,p) basis set to ensure that the optimized structures are free of imaginary vibrational frequencies and have minimal energy. To ensure the accuracy of non-covalent interactions between gas molecules and the carbon surface [32,33], dispersion corrections were also considered in the calculations [34]. The higher-precision B3LYP/6-311G(d,p) computational method was employed to obtain the single-point energy of each structure, which was used for adsorption energy calculations.

The adsorption energy during the adsorption process was calculated using Eq. (4):

$$E_{ad} = E_{complex} - E_{gas} - E_{model} \tag{4}$$

where $E_{ad}$ represents the adsorption energy (kJ·mol$^{-1}$). $E_{complex}$, $E_{gas}$, and $E_{model}$ respectively represent the single-point energies (kJ·mol$^{-1}$) of the adsorption configuration formed after gas molecule adsorption, the gas molecule, and the carbonaceous model.

The Reduced Density Gradient (RDG) method [35] is one of the techniques for visualizing weak interactions in research. It highlights areas in the system involving weak interactions, providing an intuitive understanding of which regions in the molecule are associated with weak interactions. Weak interaction analysis [36] in this study was conducted using Multiwfn software [37], and the visualization of relevant graphics was accomplished using VMD software [38].

## 3. Results and discussion

### 3.1. Adsorption characteristics of activated carbon on NO in the low-temperature range

Adsorption experiments of activated carbon in NO atmosphere were conducted at −20, −10, 0, 10, 20, and 30 °C, and the adsorption capacities at 120 min are shown in Table 3. As the temperature decreases, the adsorption capacity of activated carbon for NO slightly increases. Within the temperature range of −20 to 30 °C, the adsorption capacity of activated carbon for NO ranges from 0.0050 to 0.0055 mmol/g, indicating that there are very few adsorption sites for NO on the activated

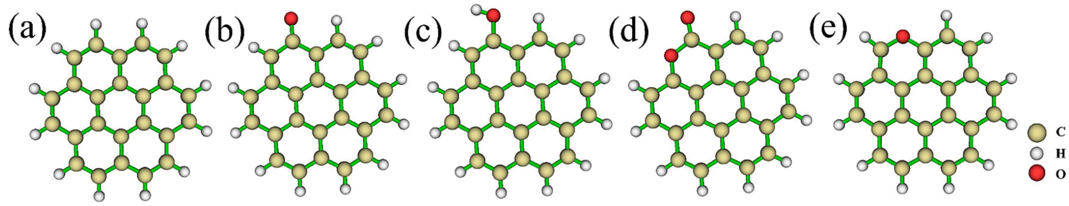


**Fig. 4.** (a) pristine carbonaceous model, (b) carbonaceous models containing carbonyl functional group, (c) hydroxyl functional group, (d) lactone functional group, and (e) ether functional group.

**Table 3**
Adsorption amount of activated carbon for $NO_x$ after 120 min of adsorption under different adsorption atmospheres (mmol/g).

| Temperature / °C | 200 ppm NO | 200 ppm NO + 5 %$O_2$ | 200 ppm $NO_2$ |
|---|---|---|---|
| 30 | 0.0050 | 0.28 | 1.26 |
| 20 | 0.0051 | 0.42 | 1.38 |
| 10 | 0.0051 | 0.62 | 1.53 |
| 0 | 0.0051 | 0.89 | 1.74 |
| −10 | 0.0052 | 1.24 | 2.05 |
| −20 | 0.0055 | 1.57 | 2.16 |

carbon.

Experiments on the adsorption of activated carbon under NO and $O_2$ atmospheres were conducted within the same temperature range. During the adsorption process, NO and $NO_2$ were detected in the reactor outlet gas. The concentration of NO and $NO_2$ in the outlet gas changed over time, as shown in Fig. 5. In Fig. 5, the concentration of NO in the outlet gas exhibits a trend of initial acceleration, followed by deceleration, then acceleration again, and finally deceleration at different temperatures. However, the concentration of $NO_2$ in the outlet gas remains very low during the 120-minute adsorption process, considering the detection limit of FTIR. It can be assumed that only at the later stage of the adsorption experiment at −20 °C, $NO_2$ was observed with a concentration of only a few ppm, showing a slowly increasing trend over time. As the adsorption temperature decreases, the outlet concentration of NO decreases. When the adsorption time reaches 120 min, the NO concentration decreases from 185.8 ppm at 30 °C to 139.7 ppm at −20 °C, indicating that low temperature favors the adsorption and conversion of NO on the surface of activated carbon. Additionally, the time at which the NO concentration reaches its maximum value occurs earlier as the adsorption temperature decreases. Referring to existing literature, the explanation for the occurrence of a maximum value in the NO breakthrough curve is that $NO_x$ adsorbed on the surface of activated carbon is released again to generate NO. This indicates that as the adsorption temperature decreases, the reaction of $NO_x$ desorption and subsequent generation of NO on the surface of activated carbon also accelerates [11].

The adsorption amounts of activated carbon for $NO_x$ within 120 min at each temperature are shown in Table 3. As the temperature decreases, the adsorption amount of activated carbon increases from 0.28 mmol/g at 30 °C to 1.57 mmol/g at −20 °C, with an increase of 1.29 mmol/g or 4.61 times. Lowering the temperature significantly promotes the adsorption of $NO_x$ on activated carbon.

To more comprehensively investigate the adsorption characteristics of activated carbon at low temperatures, an adsorption experiment of 600 min was conducted at −20 °C. During this period, the activated carbon reached saturation in adsorbing $NO_x$, and the changes in NO and $NO_2$ concentrations in the outlet gas over time are shown in Fig. 6. In Fig. 6, at −20 °C, the NO concentration in the outlet gas shows a trend of first accelerating, then decelerating, followed by accelerating again, and then decelerating. By 580 min of adsorption, the NO outlet concentration reaches 158.1 ppm, after which it remains almost unchanged. In the initial stages of adsorption, the $NO_2$ concentration in the outlet gas is very low, and it is not until 70 min later that the $NO_2$ concentration rises to a few ppm. Subsequently, the $NO_2$ outlet concentration shows a trend

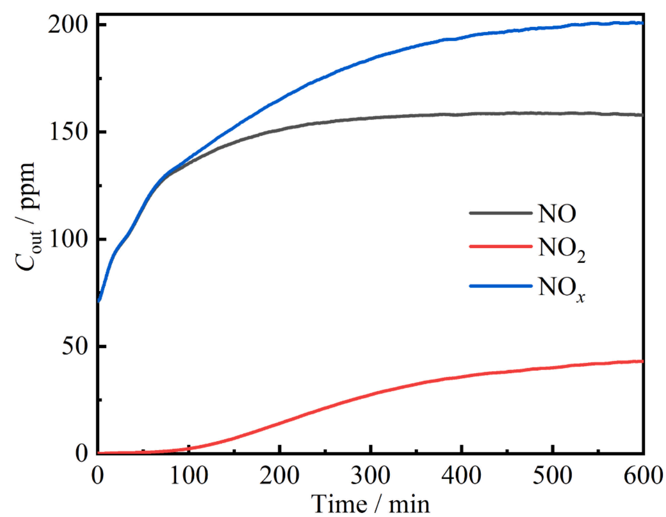


**Fig. 6.** Variation of NO and $NO_2$ outlet concentrations with time during the adsorption process of activated carbon at −20 °C (inlet concentration: 200 ppm NO and 5 % $O_2$).

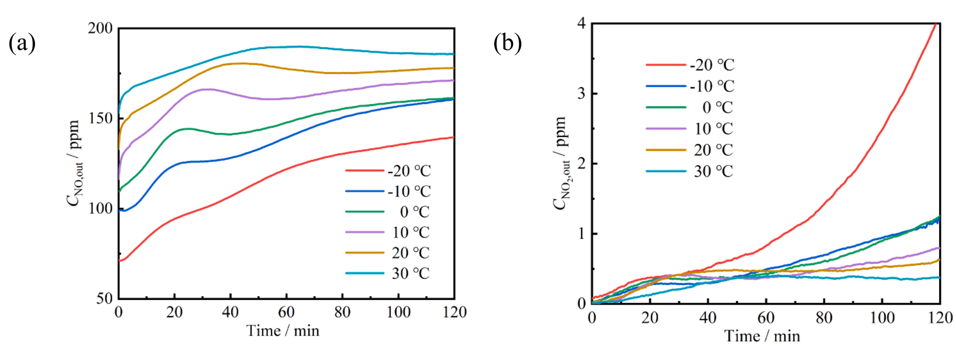


**Fig. 5.** Variation of outlet concentrations of (a) NO and (b) $NO_2$ with time during NO + $O_2$ adsorption at different adsorption temperatures.

of first accelerating, then decelerating in its increase. By 580 min of adsorption, the $NO_2$ outlet concentration reaches 42.7 ppm, after which it remains almost unchanged. At this point, the total concentration of $NO_x$ in the outlet is 200.8 ppm, which is essentially the same as the 200 ppm NO concentration in the inlet gas. This indicates that the activated carbon has reached saturation by 580 min of adsorption. At this time, the oxidation rate of NO is 21.4 %, and the adsorption capacity of activated carbon for $NO_x$ is 2.41 mmol/g. The increasing trend in NO outlet concentration shows an initial rapid rise followed by a slower increase and then another acceleration. The initial rapid rise is attributed to the gradual saturation of NO adsorption sites on the surface of the activated carbon. Subsequently, the rate of increase in NO outlet concentration slows down because the adsorbed NO continues to be oxidized to $NO_2$. The $NO_2$ generated by oxidation can desorb, allowing some sites to release and subsequently adsorb NO again. The subsequent acceleration in NO outlet concentration indicates the presence of a reaction where surface-adsorbed $NO_x$ is released from the activated carbon, generating NO [11]. As the rate of this reaction gradually decreases, the increase in NO outlet concentration slows down until it stabilizes. The presence of both NO and $NO_2$ in the outlet gas indicates that activated carbon can catalytically oxidize NO to $NO_2$ at low temperatures.

Similarly, adsorption experiments of activated carbon under $NO_2$ atmosphere were conducted within the temperature range of −20 to 30 °C. The adsorption capacities are shown in Table 3. As the adsorption temperature decreases, the adsorption amount of $NO_2$ significantly increases. The adsorption capacity of $NO_2$ on the activated carbon within this temperature range is 1.26–2.16 mmol/g, indicating significant adsorption of $NO_2$ and suggesting the presence of numerous $NO_2$ adsorption sites on the activated carbon. Additionally, since the adsorption amount of $NO_2$ is comparable to that of NO + $O_2$, it suggests that in the presence of $O_2$ during NO + $O_2$ adsorption, NO is converted to $NO_2$, leading to a substantial increase in the adsorption capacity due to the significant adsorption of generated $NO_2$ on the activated carbon.

### *3.2. Analysis of $NO_x$ desorption behavior and adsorption pathways*

After the adsorption experiments, desorption experiments were conducted on the activated carbon samples ($AC_{NO+O_2}$) obtained under different temperatures. Based on the changes in the outlet concentrations of NO and $NO_2$ during the adsorption process, desorption stage 1, and desorption stage 2, the total adsorption amount, physical adsorption amount, and chemical adsorption amount of activated carbon at different temperatures can be calculated. These are depicted in Fig. 7, represented by solid black, blue, and red lines, respectively. The sum of physical and chemical adsorption amounts represents the total $NO_x$ desorption, indicated by the black dashed line. The total amount of $NO_x$ (the sum of physical and chemical adsorption) desorbed from activated carbon is within a 5 % deviation of the total amount of $NO_x$ adsorbed by the activated carbon. This indicates that the desorption process is relatively complete. As the adsorption temperature decreases, the adsorption amount of activated carbon for $NO_x$ shows a gradually accelerating growth trend. Both the physical and chemical adsorption of $NO_x$ on activated carbon increase monotonically. The physical adsorption of activated carbon exhibits a gradually accelerating growth trend, while the chemical adsorption shows a rapid increase followed by a slower growth rate, eventually reaching a plateau. As the temperature decreases from 30 °C to −20 °C, the amount of $NO_x$ adsorbed through physical adsorption increases by 0.71 mmol/g, while the amount adsorbed through chemical adsorption increases by 0.51 mmol/g. This indicates that the significant increase in NO adsorption due to temperature reduction is correlated with the growth of both physical and chemical adsorption of $NO_x$. However, the contribution of the increase in physical adsorption of $NO_x$ is greater.

The activated carbon samples obtained after adsorption for 120 min at different temperatures underwent the desorption stage 1 experiments.

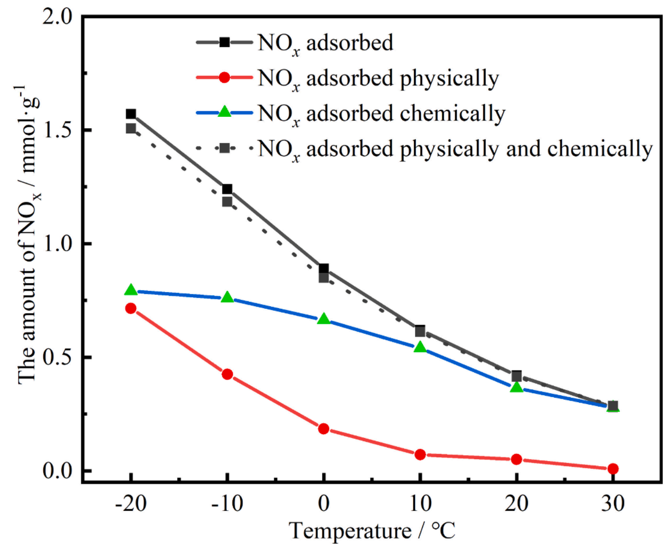


**Fig. 7.** Variation of adsorption amount, physical adsorption, and chemical adsorption of $NO_x$ by activated carbon after adsorption in NO + $O_2$ atmosphere for 120 min with temperature changes.

The nitrogen components in the desorbed gas were NO and $NO_2$, and their respective desorption amounts as well as the total physical adsorption amounts are shown in Table 4. Because the gases desorbed in the first stage are all $NO_x$ physically adsorbed, there is no conversion between them during desorption. Therefore, the desorption amounts of NO and $NO_2$ in this process can be considered as the physical adsorption amounts of NO and $NO_2$. From Table 4, it can be observed that as the adsorption temperature decreases, the physical adsorption amounts of $NO_x$, NO, and $NO_2$ all increase, especially noticeably below zero degrees. The proportion of $NO_2$ physically adsorbed on the activated carbon to the total physical adsorption amount increases as the adsorption temperature decreases. When the adsorption temperature is between 0 and 30 °C, the proportion of $NO_2$ physically adsorbed on the activated carbon to the total physical adsorption amount ranges from 0.0 % to 26.5 %. However, when the adsorption temperature is −10 and −20 °C, the proportion of $NO_2$ physically adsorbed on the activated carbon to the total physical adsorption amount is 58.6 % and 71.6 %, respectively. This indicates that lowering the adsorption temperature facilitates the oxidation of NO to $NO_2$ on the surface of the activated carbon. The physical adsorption capacity of $NO_2$ is much stronger than that of NO, so the physical adsorption of $NO_2$ on activated carbon will significantly increase at low temperatures.

The active carbon samples obtained by adsorption at different temperatures for 120 min were subjected to the second stage of the programmed temperature desorption experiment after completing the first stage desorption. The nitrogen-containing components detected in the desorption gas were NO and $NO_2$, and their desorption curves are shown in Fig. 8. In the figure, peaks of NO desorption are observed at 120, 175, and 200–500 °C, with the peak at 120 °C being the highest, followed by

**Table 4**
NO desorption, $NO_2$ desorption, and total physical adsorption of $AC_{NO+O_2}$ prepared at different temperatures during the desorption stage 1 experiment (mmol/g).

| Temperature / °C | NO | $NO_2$ | $NO_x$ (NO + $NO_2$) |
|---|---|---|---|
| 30 | 0.008 | 0.000 | 0.008 |
| 20 | 0.049 | 0.001 | 0.050 |
| 10 | 0.068 | 0.003 | 0.071 |
| 0 | 0.136 | 0.049 | 0.185 |
| −10 | 0.176 | 0.249 | 0.425 |
| −20 | 0.203 | 0.512 | 0.715 |

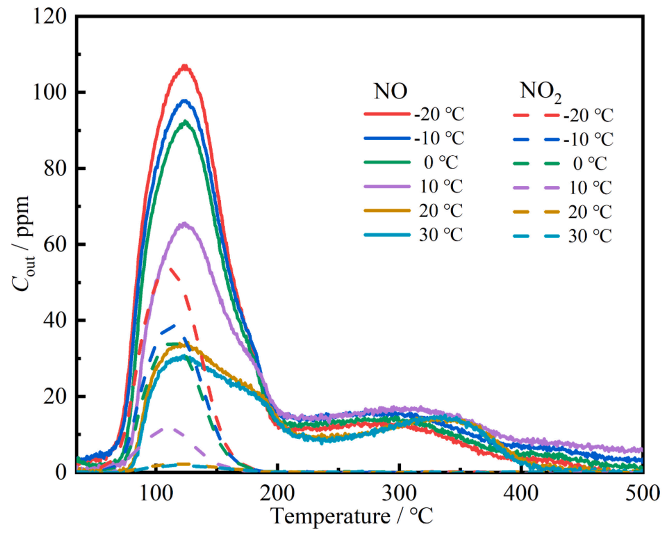


**Fig. 8.** Desorption curves of activated carbon samples obtained from adsorption at different temperatures in the desorption stage 2.

the peak at 175 °C, and the smallest peak observed at 200–500 °C. With the decrease in adsorption temperature, the peaks at 120 °C and 175 °C for desorption strengthen. The peak height at 120 °C increases from 30.6 ppm at 30 °C to 107.0 ppm at −20 °C, while the peak at 175 °C increases from 21.5 ppm at 30 °C to 37.1 ppm at −20 °C. However, there is not much change observed in the desorption peak at 200–500 °C with the variation in adsorption temperature. Peaks for $NO_2$ desorption are only observed at 110 °C. As the adsorption temperature decreases, the desorption peak for $NO_2$ increases in height, with the peak height increasing from 2.1 ppm at 30 °C to 53.4 ppm at −20 °C. As the adsorption temperature decreases, the desorption peaks for NO and $NO_2$ strengthen, indicating that lower temperatures can promote the chemical adsorption of $NO_x$ on activated carbon. The desorbed NO and $NO_2$ are generated from the breaking of $NO_x$ or nitrogen-containing functional groups adsorbed on the activated carbon. Therefore, each desorption peak can be regarded as corresponding to a certain $NO_x$ chemical adsorption configuration or nitrogen-containing functional group on the activated carbon. The desorption peaks of NO and $NO_2$ on activated carbon did not shift with changes in adsorption temperature, indicating that the $NO_x$ adsorption configurations or nitrogen-containing functional groups generated on activated carbon during NO and $O_2$ adsorption at different temperatures remain consistent. This also suggests that temperature variations do not alter the conversion pathways of $NO_x$ on activated carbon. Therefore, in conjunction with the adsorption mechanism proposed by Li et al. at 30 °C [11], the surface nitrogen species present on activated carbon corresponding to each desorption peak can be further analyzed. At low temperatures, activated carbon catalyzes the oxidation of NO to $NO_2$. Subsequently, $NO_2$ chemisorbs on the activated carbon surface, forming N-down adsorption configuration and O-down adsorption configuration of $NO_2$. Additionally, the O-down adsorption configuration of $NO_2$ further transforms into adsorbed $NO_3^-$. The NO desorption peaks at 120 and 175 °C correspond to the desorption of N-down adsorption configuration and O-down adsorption configuration of $NO_2$ on the activated carbon surface, respectively. Meanwhile, the $NO_2$ desorption at 110 °C corresponds to the decomposition and release of $NO_3^-$ on the activated carbon surface.

Based on the analysis of the physical adsorption and chemical adsorption amounts of activated carbon and the desorption curves in the low-temperature range mentioned above, combined with the mechanism proposed earlier for the adsorption and transformation of $NO_x$ on the surface of activated carbon at room temperature [11], the adsorption mechanism of activated carbon at low temperatures can be clearly defined. $O_2$ first adsorbs onto the active atoms near the hydroxyl functional groups on the surface of activated carbon. It reacts with NO in the gas phase to form $NO_2$. At this site, $NO_2$ will undergo desorption. Some of the desorbed $NO_2$ stabilizes adsorption on saturated carbon atoms and partially converts to $NO_3^-$. This adsorbed $NO_2$ and $NO_3^-$ constitute the chemical adsorption of $NO_x$ on activated carbon. The other portion of desorbed $NO_2$ exists on the surface of activated carbon through physical adsorption. From the low-temperature adsorption characteristics of activated carbon, it can be observed that lowering the temperature facilitates the oxidation of NO to $NO_2$ on the surface of activated carbon. The generated $NO_2$ can be re-adsorbed through both physical and chemical pathways, with the temperature reduction exerting a more significant promotion effect on physical adsorption. Previous studies have clarified the adsorption modes of NO near metal atoms during chemical adsorption and transformation processes, as well as the adsorption modes of $NO_2$ near nitrogen-containing components on the surface of activated carbon [11,18–22]. However, the physical adsorption configuration of $NO_x$ near oxygen-containing functional groups on the surface of activated carbon and the role of oxygen-containing functional groups remain unknown. Therefore, Section 3.3 employs density functional theory calculations to further investigate the physical adsorption of $NO_x$ on the surface of activated carbon.

### *3.3. Density functional theory calculations of $NO_x$ physical adsorption on activated carbon*

This section calculates the physical adsorption of NO and $NO_2$ on the pristine carbonaceous model and the carbonaceous model containing carbonyl, ether, hydroxyl, and lactone groups. The physical adsorption configurations of NO and $NO_2$ are depicted in Figs. 9 and 10, respectively.

On the pristine carbonaceous model, NO can physically adsorb on the edges and basal plane of the carbonaceous model, as shown in Fig. 9a and b, with adsorption energies of −4.0 and −6.1 kJ/mol, respectively. On the carbonaceous model containing carbonyl, ether, and hydroxyl groups, NO can physically adsorb on the basal plane of the carbonaceous model. On the carbonaceous model containing lactone groups, NO can physically adsorb on the edges of the carbonaceous model, as depicted in Fig. 9c–f, with adsorption energy ranging from −5.2 to + 44.5 kJ/mol.

On the pristine carbonaceous model, $NO_2$ can physically adsorb on the edges and basal plane of the carbonaceous model, as shown in Fig. 10a and b, with adsorption energies of −81.4 and −73.1 kJ/mol, respectively. On the carbonaceous model containing carbonyl, ether, and hydroxyl groups, $NO_2$ can physically adsorb on the basal plane of the carbonaceous model. On the carbonaceous model containing lactone groups, $NO_2$ can physically adsorb on the edges of the carbonaceous model, as depicted in Fig. 10c–f, with adsorption energies of −38.5, −77.5, −78.8, and −82.7 kJ/mol, respectively. In the two adsorption configurations of $NO_2$ on the pristine carbonaceous model, edge adsorption of $NO_2$ is more stable than basal plane adsorption of $NO_2$. This suggests that $NO_2$ is more likely to adsorb on the edges of the carbonaceous model when in proximity to activated carbon. Concerning the four oxygen-containing functional groups present on activated carbon, it is observed that the presence of carbonyl groups is detrimental to the physical adsorption of $NO_2$ on the basal plane of activated carbon. However, the presence of ether and hydroxyl groups can enhance the stability of $NO_2$ physical adsorption on the basal plane of activated carbon, while the presence of lactone groups can enhance the stability of $NO_2$ physical adsorption on the edges of activated carbon. Comparing the physical adsorption energies of NO and $NO_2$, it is noted that the physical adsorption energy of $NO_2$ is significantly smaller than that of NO, indicating that the physical adsorption capacity of $NO_2$ on the activated carbon surface is much stronger than that of NO.

The non-covalent interactions of physical adsorption configurations of $NO_2$ on the activated carbon were analyzed using the RDG function to explore the adsorption interactions between $NO_2$ and the carbonaceous model. Fig. 11 shows the gradient isosurfaces of the RDG function for the

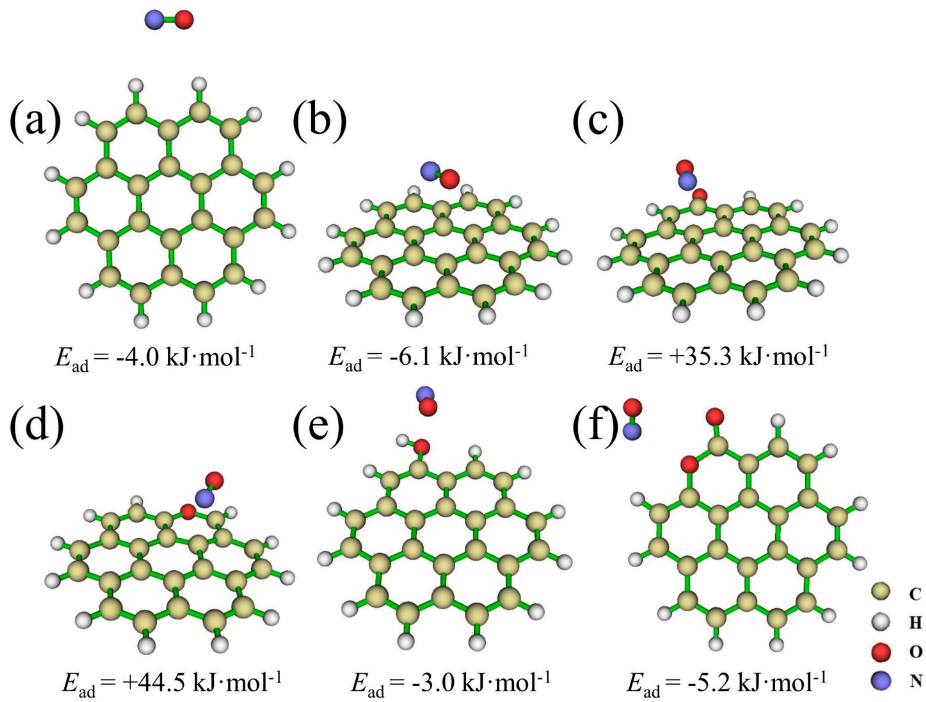


**Fig. 9.** Physical adsorption configurations of NO on activated carbon. NO adsorption configurations adsorbed on the (a) edges and (b) basal plane of the pristine carbonaceous model, NO adsorption configurations on carbonaceous models containing (c) carbonyl, (d) ether groups, (e) hydroxyl groups, and (f) lactone groups.

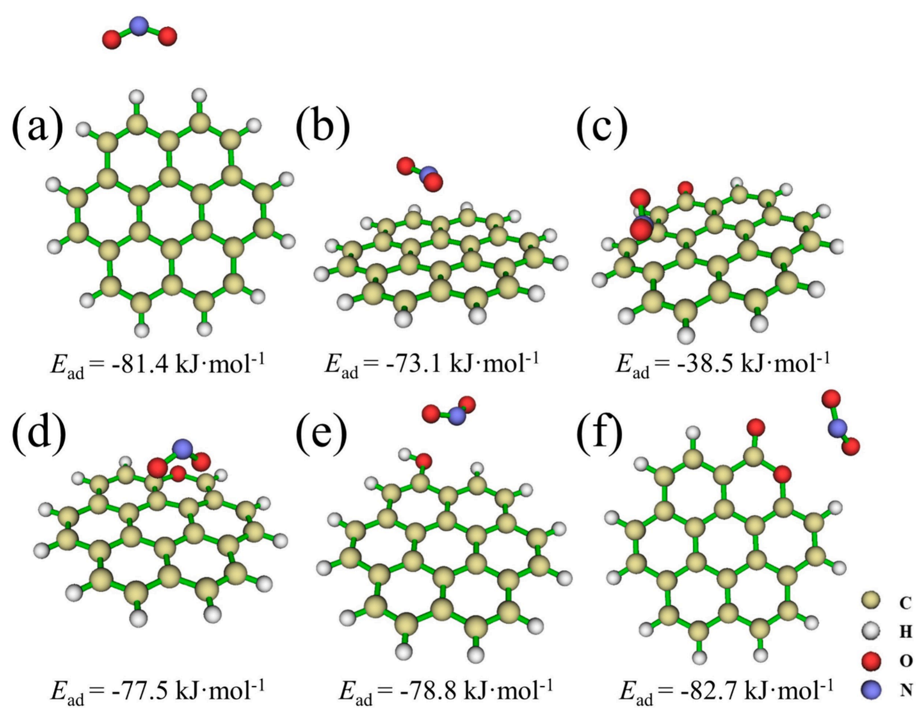


**Fig. 10.** Physical adsorption configurations of $NO_2$ on activated carbon. $NO_2$ adsorption configurations adsorbed on the (a) edges and (b) basal plane of the pristine carbonaceous model, $NO_2$ adsorption configurations on carbonaceous models containing (c) carbonyl, (d) ether groups, (e) hydroxyl groups, and (f) lactone groups.

six adsorption configurations, where the isosurfaces of the RDG function ($s = 0.5$ a.u.) are colored according to the sign($\lambda_2$)$\rho$ value. The color range varies from blue-green to red, with a distribution range of −0.04 to 0.02 a.u. In Fig. 12, the corresponding scatter plots are presented. In the contour plots of the RDG function, the green contour surface corresponds to peaks near zero (−0.02 to 0.02 a.u.), representing weak van der Waals interactions. The blue contour surface corresponds to peaks with large negative values (−0.04 to −0.02 a.u.), indicating strong attractive interactions such as hydrogen bonding or halogen bonding. The red peaks correspond to peaks with large positive values (0.02 a.u.), representing steric effects from rings or cages, exhibiting strong repulsive interactions.

In Fig. 11, for the six adsorption configurations of $NO_2$, it can be observed that there are red diamond structures present in all six-

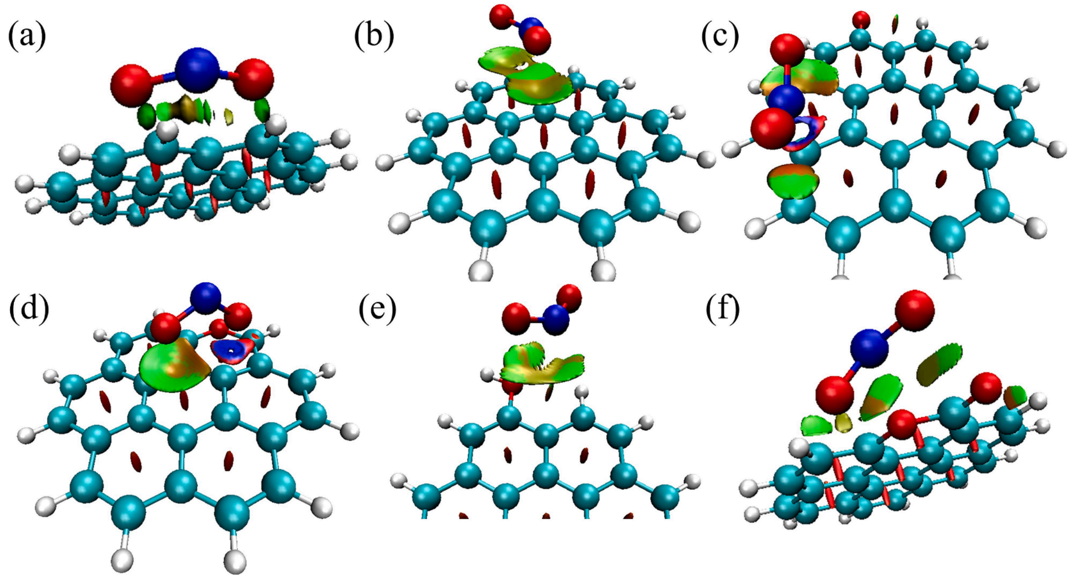


**Fig. 11.** Gradient isosurfaces for $NO_2$ adsorption configurations on the (a) edges and (b) basal plane of the pristine carbonaceous model, on carbonaceous models containing (c) carbonyl, (d) ether groups, (e) hydroxyl groups, and (f) lactone groups.

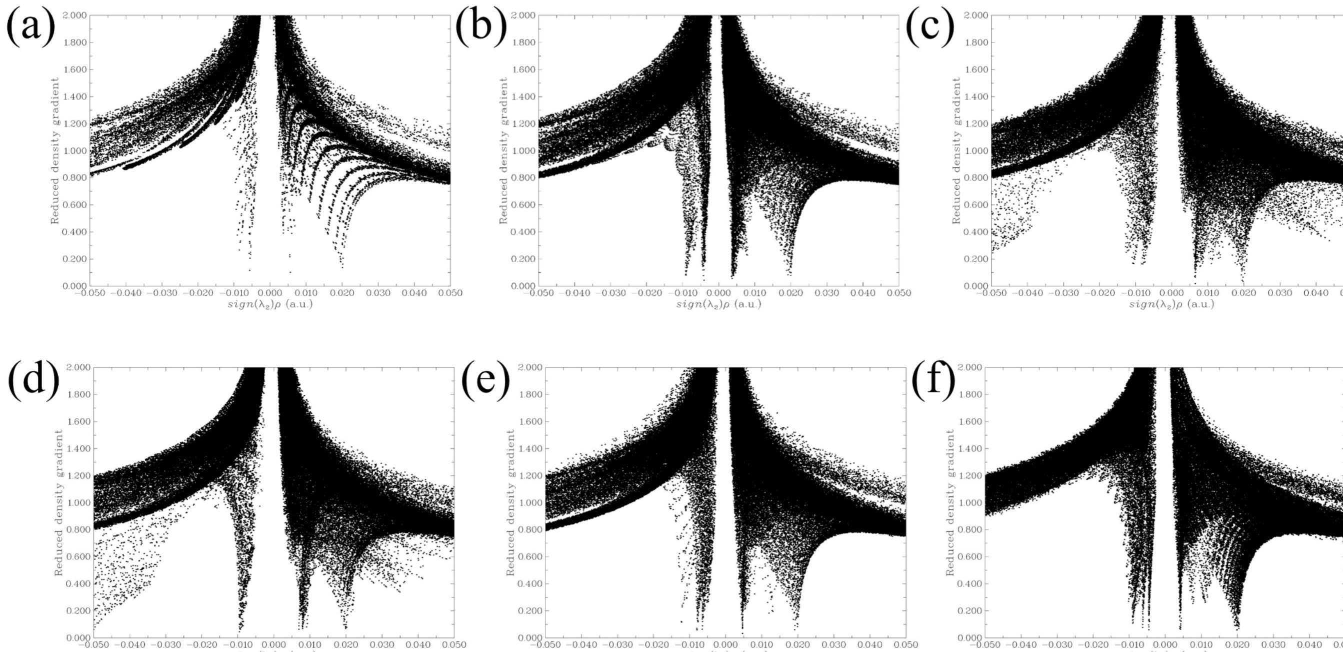


**Fig. 12.** Scatter plots of sign($\lambda_2$)$\rho$ and RDG for $NO_2$ adsorption configurations on the (a) edges and (b) basal plane of the pristine carbonaceous model, on carbonaceous models containing (c) carbonyl, (d) ether groups, (e) hydroxyl groups, and (f) lactone groups.

membered carbon rings, corresponding to the peaks at 0.02 a.u. in Fig. 12, representing steric effects of the six-membered rings. Fig. 11a and b depict the two adsorption configurations of $NO_2$ on the original carbonaceous model. In these configurations, both green and brown contour surfaces are observed between $NO_2$ and the carbonaceous model. The green contour corresponds to peaks in the range of −0.01 to 0 a.u. in Fig. 12a and b, indicating weak hydrogen bonding effects, representing weak attractive interactions. The brown contour corresponds to peaks in the range of 0 to 0.01 a.u. in Fig. 12a and b, indicating weak steric effects, representing weak repulsive interactions. This suggests that the interaction between $NO_2$ and the original carbonaceous model is primarily governed by weak van der Waals interactions. Fig. 11c–f illustrate the adsorption configurations of $NO_2$ on carbonaceous models containing carbonyl, ether, hydroxyl, and lactone groups. In these four configurations, similar green and brown contour surfaces are observed between $NO_2$ and the carbonaceous model, representing weak hydrogen bonding effects and weak steric effects, respectively, indicative of van der Waals interactions.

Density functional theory calculations on the physical adsorption of $NO_2$ on activated carbon reveal that $NO_2$ can physically adsorb on the edge or basal plane of the original carbonaceous model, with a preference for adsorption on the edge. The presence of carbonyl groups on activated carbon is unfavorable for the physical adsorption of $NO_2$ on the basal plane, while the presence of ether and hydroxyl groups facilitates the physical adsorption of $NO_2$ on the basal plane. The presence of lactone groups favors the physical adsorption of $NO_2$ on the edge.

Additionally, the physical adsorption capacity of $NO_2$ on the surface of activated carbon is much stronger than that of NO. The physical adsorption of $NO_2$ on the carbonaceous model is primarily governed by relatively weak van der Waals interactions between $NO_2$ and activated carbon.

At low temperatures, the active sites for NO oxidation are the active atoms near the hydroxyl functional groups on the surface of activated carbon, where NO can be continuously oxidized to $NO_2$. The oxidized $NO_2$ undergoes desorption and can physically or chemically adsorb onto other sites on the activated carbon surface. Previous studies [11] have indicated that the active sites for the chemical adsorption of $NO_2$ are saturated carbon atoms, where $NO_2$ can chemically adsorb and some of it can be converted to $NO_3^-$. However, our research findings suggest that the active sites for the physical adsorption of $NO_2$ are near saturated carbon atoms and oxygen-containing functional groups. Surface modification techniques can be employed to increase the presence of ether, hydroxyl, and lactone functional groups on the activated carbon surface, thereby increasing the number of active sites for NO oxidation and enhancing the physical adsorption of $NO_2$. This enhancement ultimately improves the low-temperature adsorption performance of activated carbon for NO.

## 4. Conclusion

At low temperatures (−20 to 30 °C), activated carbon exhibits very weak adsorption of NO without the presence of $O_2$, while it strongly adsorbs $NO_2$. In the presence of $O_2$, activated carbon catalyzes the oxidation of NO, resulting in a 56- to 285-fold increase in $NO_x$ adsorption, comparable to the adsorption of $NO_2$. Under a 200 ppm NO + 5 % $O_2$ atmosphere, the adsorption capacity of activated carbon increases from 0.28 mmol/g at 30 °C to 1.57 mmol/g at −20 °C, a 4.61-fold increase. Lowering temperatures significantly enhance $NO_x$ adsorption. Saturation adsorption experiments at −20 °C reveal that the activated carbon surface undergoes both the oxidation of NO to $NO_2$ and the reduction of adsorbed $NO_x$ to NO during the adsorption process.

Desorption experiments were conducted for activated carbon samples adsorbed with NO and $O_2$ at different temperatures. As the adsorption temperature decreases, the amount of physically adsorbed $NO_x$ on the activated carbon gradually increases, while the amount of chemically adsorbed $NO_x$ shows a rapid increase followed by slow growth and eventual stabilization. The increase in physically adsorbed $NO_x$ is more significant. Lower temperatures favor the oxidation of NO on the activated carbon surface, and it is also found that $NO_2$ has a stronger physical adsorption capacity compared to NO. Furthermore, the temperature corresponding to the desorption peak of the adsorbed activated carbon remained unchanged, suggesting that adsorption temperature variations do not alter the conversion pathways of $NO_x$ on the activated carbon.

Density functional theory calculations were conducted to investigate the physical adsorption configurations of $NO_x$ on activated carbon. The physical adsorption energy of NO on the activated carbon surface ranged from −5.2 to + 44.5 kJ/mol, while that of $NO_2$ ranged from −82.7 to −38.5 kJ/mol, indicating that $NO_2$ has a much stronger physical adsorption capacity compared to NO. $NO_2$ was found to physically adsorb near saturated carbon atoms and oxygen-containing functional groups. The presence of carbonyl groups on the activated carbon was unfavorable for $NO_2$ physical adsorption, whereas the presence of ether, hydroxyl, and lactone groups promoted $NO_2$ physical adsorption. Reduced density gradient analysis revealed that the interaction between physically adsorbed $NO_2$ and activated carbon is primarily characterized by relatively weak van der Waals interactions.

During low-temperature adsorption, NO is first oxidized to $NO_2$ at active sites near hydroxyl functional groups. Subsequently, a portion of $NO_2$ chemisorbs onto saturated carbon atoms, while another portion physisorbs near saturated carbon atoms and oxygen-containing functional groups. The mechanism of NO low-temperature adsorption on activated carbon elucidated in this study can guide the modification of activated carbon and the optimization of low-temperature adsorption techniques.

## CRediT authorship contribution statement

**Zhongwei Li:** Writing – review & editing, Writing – original draft, Visualization, Validation, Software, Methodology, Investigation, Data curation, Conceptualization. **Xingyu Yang:** Writing – review & editing, Validation, Methodology, Data curation, Conceptualization. **Yutong Wang:** Validation, Supervision, Resources. **Hairui Yang:** Writing – review & editing, Validation, Supervision. **Qiang Song:** Writing – review & editing, Supervision, Methodology, Conceptualization.

## Declaration of competing interest

The authors declare that they have no known competing financial interests or personal relationships that could have appeared to influence the work reported in this paper.

## Data availability

Data will be made available on request.

## Acknowledgements

This work was supported by the National Key Research and Development Program of China (2022YFB4100201), National Natural Science Foundation of China (51976103) and the Fundamental Research Funds for the Central Universities of China (2022ZFJH04).

## References

[1] J. Yang, G. Mestl, D. Herein, R. Schlögl, J. Find, Reaction of NO with carbonaceous materials: 1 reaction and adsorption of NO on Ashless carbon black, Carbon 38 (5) (2000) 715–727, https://doi.org/10.1016/S0008-6223(99)00150-5.
[2] Z.-Z. Wang, R. Sun, T.M. Ismail, J. Xu, X.-Z. Zhang, Y.-P. Li, Characterization of coal char surface behavior after a heterogeneous oxidative treatment, Fuel 210 (2017) 154–164, https://doi.org/10.1016/j.fuel.2017.08.030.
[3] M. Jeguirim, M. Belhachemi, L. Limousy, S. Bennici, Adsorption/reduction of nitrogen dioxide on activated carbons: textural properties versus surface chemistry – a review, Chem. Eng. J. 347 (2018) 493–504, https://doi.org/10.1016/j.cej.2018.04.063.
[4] S.I. Anthonysamy, P. Lahijani, M. Mohammadi, A.R. Mohamed, Alkali-modified biochar as a sustainable adsorbent for the low-temperature uptake of nitric oxide, Int. J. Environ. Sci. Technol. 19 (8) (2022) 7127–7140, https://doi.org/10.1007/s13762-021-03617-3.
[5] S. Wang, S. Xu, S. Gao, P. Xiao, M. Jiang, H. Zhao, B. Huang, L. Liu, H. Niu, J. Wang, D. Guo, Simultaneous removal of $SO_2$ and $NO_x$ from flue gas by low-temperature adsorption over activated carbon, Sci. Rep. 11 (1) (2021) 11003, https://doi.org/10.1038/s41598-021-90532-9.
[6] A. Claudino, J.L. Soares, R. Moreira, H.J. Jose, Adsorption equilibrium and breakthrough analysis for NO adsorption on activated carbons at low temperatures, Carbon 42 (8–9) (2004) 1483–1490, https://doi.org/10.1016/j.carbon.2004.01.048.
[7] B. Li, L. Zhang, Z. Wang, C. Ma, NO Adsorption over Powder Activated Carbon in a Fluidized Bed, Asia-Pacific Power and Energy Engineering Conference 2011 (2011) 1–4.
[8] D. Lopez, R. Buitrago, A. Sepulveda-Escribano, F. Rodriguez-Reinoso, F. Mondragon, Low-temperature catalytic adsorption of NO on activated carbon materials, Langmuir 23 (24) (2007) 12131–12137, https://doi.org/10.1021/la701501q.
[9] S.A. Dastgheib, H. Salih, T. Ilangovan, J. Mock, NO oxidation by activated carbon catalysts: impact of carbon characteristics pressure, and the presence of water, Acs Omega 5 (33) (2020) 21172–21180, https://doi.org/10.1021/acsomega.0c02891.
[10] X. Zhu, L. Zhang, T. Wang, J. Li, X. Zhou, C. Ma, Y. Dong, An updated study on NO catalytic oxidation over activated carbon: the effect of pore structure and a dual-site mechanism, Fuel 311 (2022) 122627, https://doi.org/10.1016/j.fuel.2021.122627.
[11] Z. Li, G. Song, X. Yang, Q. Song, Mechanism of $O_2$-promoted NO adsorption on activated carbon: an experimental and computational study, Chem. Eng. J. 481 (2024) 148391, https://doi.org/10.1016/j.cej.2023.148391.
[12] Q. Feng, J. Zhang, C. Peng, Z. Cai, Synthesis of modified sludge biochar for flue gas denitration: biochar properties, synergistic efficiency and mechanism, Waste Manag. 170 (2023) 204–214, https://doi.org/10.1016/j.wasman.2023.08.007.

[13] Z. Zhang, J.D. Atkinson, B. Jiang, M.J. Rood, Z. Yan, Nitric oxide oxidation catalyzed by microporous activated carbon fiber cloth: an updated reaction mechanism, Appl Catal B 148–149 (2014) 573–581, https://doi.org/10.1016/j.apcatb.2013.10.050.

[14] Z. Xu, Y. Li, J. Guo, J. Xiong, Y. Lin, T. Zhu, An efficient and sulfur resistant K-modified activated carbon for SCR denitrification compared with acid- and Cu-modified activated carbon, Chem. Eng. J. 395 (2020) 125047, https://doi.org/10.1016/j.cej.2020.125047.

[15] F.-T. You, G.-W. Yu, Z.-J. Xing, J. Li, S.-Y. Xie, C.-X. Li, G. Wang, H.-Y. Ren, Y. Wang, Enhancement of NO catalytic oxidation on activated carbon at room temperature by nitric acid hydrothermal treatment, Appl. Surf. Sci. 471 (2019) 633–644, https://doi.org/10.1016/j.apsusc.2018.12.066.

[16] R. Zhang, F. Gao, X. Tang, H. Yi, Y. Zhou, Temperature responses of two synergistic pathways for low-temperature catalytic oxidation of high-concentration NO over ACFs: nano-confinement and nitrogen-containing groups, Fuel 325 (2022) 124878, https://doi.org/10.1016/j.fuel.2022.124878.

[17] D. Wang, J. Pan, D. Zhu, Z. Guo, C. Yang, X. Duan, Enhanced adsorption of NO onto activated carbon by gas pre-magnetization, Sci. Total Environ. 830 (2022) 154712, https://doi.org/10.1016/j.scitotenv.2022.154712.

[18] X. Wang, R. Yao, Z. Bai, H. Ma, The active sites and mechanism of NO oxidation on modified activated carbon, React. Kinet. Mech. Catal. 120 (1) (2017) 209–217, https://doi.org/10.1007/s11144-016-1091-9.

[19] X. Zhang, R. Lin, Effect of alkali metal elements on nitric oxide chemisorption at the edge of char: a DFT study, Innovat. Sol. Energy Trans. 158 (2019) 4805–4809, https://doi.org/10.1016/j.egypro.2019.01.716.

[20] J. Yang, S. Yuan, S. Wang, M. Yang, B. Shen, Q. Zhang, Z. Zhang, F. Wang, L. Xu, Z. Wang, Density functional theory study on the effect of sodium on the adsorption of NO on a char surface, Energy Fuel 34 (7) (2020) 8726–8731, https://doi.org/10.1021/acs.energyfuels.0c00987.

[21] L. Chen, J. Yang, M. Zhang, M. Gao, J. Su, Y. Huang, Z. Zhang, Z. Wang, L. Xu, B. Shen, Theoretical study of NO adsorption by hydroxyl-containing char with the participation of Na/K, Langmuir 38 (32) (2022) 9940–9954, https://doi.org/10.1021/acs.langmuir.2c01244.

[22] X. Zhu, L. Zhang, M. Zhang, C. Ma, Effect of N-doping on $NO_2$ adsorption and reduction over activated carbon: an experimental and computational study, Fuel 258 (2019) 116109, https://doi.org/10.1016/j.fuel.2019.116109.

[23] Y. Guo, Y. Li, T. Zhu, M. Ye, Effects of concentration and adsorption product on the adsorption of $SO_2$ and NO on activated carbon, Energy Fuel 27 (1) (2013) 360–366, https://doi.org/10.1021/ef3016975.

[24] K. Zhang, Y. He, Z. Wang, T. Huang, Q. Li, S. Kumar, K. Cen, Multi-stage semi-coke activation for the removal of $SO_2$ and NO, Fuel 210 (2017) 738–747, https://doi.org/10.1016/j.fuel.2017.08.107.

[25] A.P. Terzyk, The influence of activated carbon surface chemical composition on the adsorption of acetaminophen (paracetamol) in vitro: Part II. TG, FTIR, and XPS analysis of carbons and the temperature dependence of adsorption kinetics at the neutral pH, Colloids and Surfaces A: Physicochemical and Engineering Aspects 177 (1) (2001) 23-45. https://doi.org/10.1016/S0927-7757(00)00594-X.

[26] J. Wang, M. Yang, D. Deng, S. Qiu, The adsorption of NO, $NH_3$, $N_2$ on carbon surface: a density functional theory study, J. Mol. Model. 23 (9) (2017) 262, https://doi.org/10.1007/s00894-017-3429-2.

[27] X. Pi, F. Sun, J. Gao, Z. Qu, A. Wang, Z. Qie, L. Wang, H. Liu, A new insight into the $SO_2$ adsorption behavior of oxidized carbon materials using model adsorbents and DFT calculations, PCCP 21 (18) (2019) 9181–9188, https://doi.org/10.1039/c8cp07782g.

[28] Z. Qu, F. Sun, J. Gao, X. Pi, Z. Qie, G. Zhao, A new insight into $SO_2$ low-temperature catalytic oxidation in porous carbon materials: non-dissociated O-2 molecule as oxidant, Cat. Sci. Technol. 9 (16) (2019) 4327–4338, https://doi.org/10.1039/c9cy00960d.

[29] Z. Li, W. Zhang, Z. Chen, Q. Zhang, X. Yang, S. Mao, W. Jian, Reaction mechanism for NO oxidation on the soot surface using a quantum chemistry, Fuel 313 (2022) 123032, https://doi.org/10.1016/j.fuel.2021.123032.

[30] Z. Qu, F. Sun, X. Pi, X. Li, D. Wu, J. Gao, G. Zhao, One-step synergistic optimization of hierarchical pore topology and nitrogen dopants in activated coke for efficient catalytic oxidation of nitric oxide, J. Clean. Prod. 335 (2022) 130360, https://doi.org/10.1016/j.jclepro.2022.130360.

[31] M.J. Frisch, G.W. Trucks, H.B. Schlegel, G.E. Scuseria, M.A. Robb, J.R. Cheeseman, G. Scalmani, V. Barone, G.A. Petersson, H. Nakatsuji, X. Li, M. Caricato, A.V. Marenich, J. Bloino, B.G. Janesko, R. Gomperts, B. Mennucci, H.P. Hratchian, J.V. Ortiz, A.F. Izmaylov, J.L. Sonnenberg, Williams, F. Ding, F. Lipparini, F. Egidi, J. Goings, B. Peng, A. Petrone, T. Henderson, D. Ranasinghe, V.G. Zakrzewski, J. Gao, N. Rega, G. Zheng, W. Liang, M. Hada, M. Ehara, K. Toyota, R. Fukuda, J. Hasegawa, M. Ishida, T. Nakajima, Y. Honda, O. Kitao, H. Nakai, T. Vreven, K. Throssell, J.A. Montgomery Jr., J.E. Peralta, F. Ogliaro, M.J. Bearpark, J.J. Heyd, E.N. Brothers, K.N. Kudin, V.N. Staroverov, T.A. Keith, R. Kobayashi, J. Normand, K. Raghavachari, A.P. Rendell, J.C. Burant, S.S. Iyengar, J. Tomasi, M. Cossi, J.M. Millam, M. Klene, C. Adamo, R. Cammi, J.W. Ochterski, R.L. Martin, K. Morokuma, O. Farkas, J.B. Foresman, D.J. Fox, Gaussian 16, ReVision C.01, Gaussian, Inc., Wallingford, CT, 2016.

[32] X.-Y. Liu, J.-M. Zhang, K.-W. Xu, V. Ji, Improving $SO_2$ gas sensing properties of graphene by introducing dopant and defect: a first-principles study, Appl. Surf. Sci. 313 (2014) 405–410, https://doi.org/10.1016/j.apsusc.2014.05.223.

[33] L. Ma, J.-M. Zhang, K.-W. Xu, Hydrogen storage on nitrogen induced defects in palladium-decorated graphene: a first-principles study, Appl. Surf. Sci. 292 (2014) 921–927, https://doi.org/10.1016/j.apsusc.2013.12.080.

[34] S. Grimme, J. Antony, S. Ehrlich, H. Krieg, A consistent and accurate ab initio parametrization of density functional dispersion correction (DFT-D) for the 94 elements H-Pu, J. Chem. Phys. 132 (15) (2010), https://doi.org/10.1063/1.3382344.

[35] E.R. Johnson, S. Keinan, P. Mori-Sánchez, J. Contreras-García, A.J. Cohen, W. Yang, Revealing noncovalent interactions, J. Am. Chem. Soc. 132 (18) (2010) 6498–6506, https://doi.org/10.1021/ja100936w.

[36] T. Lu, Q. Chen, Visualization analysis of weak interactions in chemical systems, comprehensive computational, Chemistry 2 (2024) 240–264, https://doi.org/10.1016/B978-0-12-821978-2.00076-3.

[37] T. Lu, F. Chen, Multiwfn: a multifunctional wavefunction analyzer, J. Comput. Chem. 33 (5) (2012) 580–592, https://doi.org/10.1002/jcc.22885.

[38] W. Humphrey, A. Dalke, K. Schulten, VMD: visual molecular dynamics, J. Mol. Graph. 14 (1) (1996) 33–38, https://doi.org/10.1016/0263-7855(96)00018-5.